HHS Public Access

Author manuscript

J Am Chem Soc. Author manuscript; available in PMC 2019 June 17.

Published in final edited form as:

J Am Chem Soc. 2018 December 12; 140(49): 17175–17187. doi:10.1021/jacs.8b09961.

Tetranuclear [$Mn^{III}Mn_3^{IV}O_4$] Complexes as Spectroscopic Models of the S_2 State of the Oxygen Evolving Complex in Photosystem II

Heui Beom Lee[†], **Angela A. Shiau**[†], **Paul H. Oyala**[†], **David A. Marchiori**[‡], **Sheraz Gul**[§], **Ruchira Chatterjee**[§], **Junko Yano**[§], **R. David Britt**[*,‡], and **Theodor Agapie**[*,†]

[†]Department of Chemistry and Chemical Engineering, California Institute of Technology, 1200 E California Blvd MC 127-72, Pasadena, CA 91125, USA

[‡]Department of Chemistry, University of California, Davis, One Shields Ave, Davis, California 95616, USA

[§]Molecular Biophysics and Integrated Bioimaging Division, Lawrence Berkeley National Laboratory, Berkeley, CA 94720, USA

Abstract

Despite extensive biochemical, spectroscopic, and computational studies, the mechanism of biological water oxidation by the Oxygen Evolving Complex (OEC) of Photosystem II remains a subject of significant debate. Mechanistic proposals are guided by the characterization of reaction intermediates such as the S_2 state, which features two characteristic EPR signals at $g = 2$ and $g = 4.1$. Two nearly isoenergetic structural isomers have been proposed as the source of these distinct signals, but relevant structure−electronic structure studies remain rare. Herein, we report the synthesis, crystal structure, electrochemistry, XAS, magnetic susceptibility, variable temperature CW-EPR, and pulse EPR data for a series of [$Mn^{III}Mn_3^{IV}O_4$] cuboidal complexes as spectroscopic models of the S_2 state of the OEC. Resembling the oxidation state and EPR spectra of the S_2 state of the OEC, these model complexes show two EPR signals, a broad low field signal and a multiline signal, that are remarkably similar to the biological system. The effect of systematic changes in the nature of the bridging ligands on spectroscopy were studied. Results show that the electronic structure of tetranuclear Mn complexes is highly sensitive to even small geometric changes and the nature of the bridging ligands. Our model studies suggest that the spectroscopic properties of the OEC may also react very sensitively to small changes in structure; the effect of protonation state and other reorganization processes need to be carefully assessed.

Graphical abstract

[*]**Corresponding Author** rdbritt@ucdavis.edu. [*] agapie@caltech.edu.

ASSOCIATED CONTENT

Supporting Information. Experimental procedures and characterization. This material is available free of charge via the Internet at http://pubs.acs.org.

Notes

The authors declare no competing financial interest.

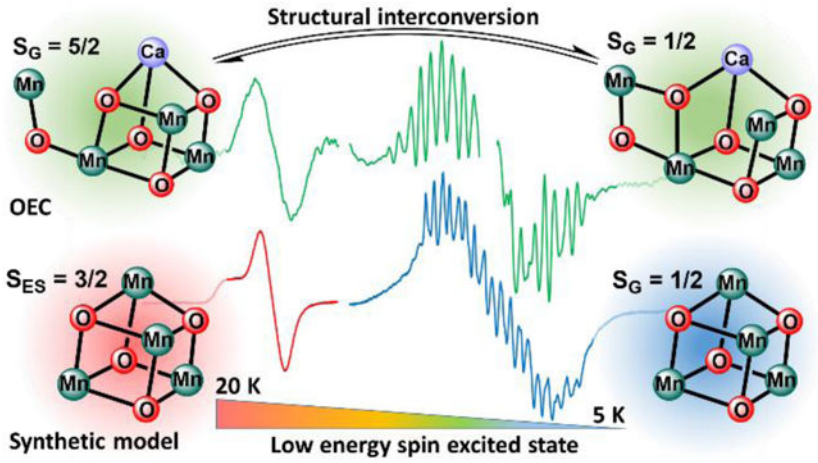

INTRODUCTION

Structural determination and spectroscopic characterization of intermediates (and derivatives thereof) in the S-state catalytic cycle of the Oxygen Evolving Complex (OEC) of Photosystem II (PSII) heavily influence mechanistic proposals for O−O bond formation.[1–14] The dark-stable S_1 state of the OEC consists of a $CaMn_4O_5$ cluster with Mn oxidation states $Mn^{III}_2Mn^{IV}_2$.[15] Light-induced one electron oxidation of the S_1 state results in the formation of the S_2 state, with two characteristic EPR transitions centered at $g = 2$ and $g = 4.1$.[9, 11, 13, 16] Two additional one electron oxidations lead to the formation of S_3 and S_4 states, respectively, and dioxygen is evolved following formation of the elusive S_4 state.[17] Chemical changes such as Ca^{2+} removal or treatment with NH_3 or F^- inhibit the $S_2 \rightarrow S_3$ transition specifically, highlighting opportunities for mechanistic insight,[4, 18] but also the need for benchmarking with well characterized synthetic models. Constrained by available data from XAS and EPR spectroscopy, the current understanding of the S_2 state structure is based on theoretical studies starting from the high-resolution (1.95 Å), radiation damage-free X-ray structure of the S_1 state.[19–20] Each EPR signal in the S_2 state is proposed to originate from different structures (Fig. 1): an “open cubane” structure with a low-spin (LS) $S = 1/2$ ground state and a “closed cubane” structure with a high-spin (HS) $S = 5/2$ ground state.[21–23] The interconvertibility of the two EPR signals suggest a small energy difference between these two structures; IR irradiation of the LS form at 120−150 K results in the formation of the HS form, which can be reverted to the LS form by annealing at 200 K.[11] The two structural isomers effectively differ only by the relative position of the bridging O(5) oxygen, a water derived oxygen, which is proposed to undergo O−O coupling to generate O_2.[24–25] Time-resolved, femtosecond X-ray free electron laser (XFEL) techniques offer the possibility of observing structural and spectroscopic changes in the OEC under dynamic, catalytically active conditions.[26–31] For such studies, further improvements in resolution and issues with S-state heterogeneity and deconvolution remain to be addressed.[27, 31–32]

Growing experimental data support that conversion from the LS form of the S_2 state to its HS form is an intermediate step in the $S_2 \rightarrow S_3$ transition.[33] pH dependence studies indicate

that deprotonation of the LS form leads to the HS form.[34] Structural changes following deprotonation are unknown, but computational studies suggest that the electronic structure of the OEC is highly sensitive to small changes in structure as reported by EPR spectroscopy.[35] Deprotonation of a Mn-bound water and/or a reorientation of a Glu residue in the S_2 state may perturb the ground spin state from LS to HS, indicating that spectroscopic properties may react very sensitively to small geometric changes that do not lead to significant changes in the total energy of the cluster.[35] EXAFS studies support structural differences between the species responsible for the $g = 2$ and the $g = 4.1$ signal, but further atomistic details are unknown.[36–37]

In contrast to the extensive studies performed on the S_2 state of the OEC, structural and spectroscopic studies of $Mn^{III}Mn_3^{IV}$ model complexes remain rare[38–40], and can be summarized as follows. The phosphinate-bridged, cuboidal complex $[Mn_4O_4(Ph_2PO_2)_6]^+$ shows a broad EPR spectrum.[41] The $g = 4.1$ signal of the adamantane-shaped complex $[Mn_4O_6(bpea)_4]^{3+}$ has been assigned to the first excited Kramers doublet of an $S = 5/2$ ground state determined from magnetization data.[42] Starting from a linear-chain precursor, a putative complex $[Mn_4O_6(bpy)_6]^{3+}$ was generated by radiolysis and features a multiline signal centered at $g = 2$ consistent with an $S = 1/2$ ground state.[43] In-situ oxidation of a close OEC structural model complex, $CaMn_4O_4(OPiv)_8$, gives rise to two EPR signals at $g = 4.9$ and $g = 2$, attributed to different spin states of the cluster corresponding to a $[CaMn_4O_4(OPiv)_8]^+$ species, although further structural, spectroscopic, and magnetic data have not been provided.[44] Follow-up computational studies disagree on the assignment of the two signals, one of them suggesting that the two signals must be due to structurally very different clusters.[45–46] In general, systematic studies that probe the effect of small structural changes on the spectroscopic and magnetic properties of S_2 model clusters are very rare, likely due to the synthetic challenges of accessing a series of isolable clusters that are suitable for comparisons.[47–48] Indeed, despite significant efforts to prepare tetra-and penta-nuclear clusters that are relevant to the S-state intermediates in terms of structure, redox state, or spectroscopy, accurate models for benchmarking against the biological system are rare.[41, 47, 49–69]

Herein, we report the synthesis, crystal structure, electrochemistry, XAS, SQUID magnetometry, variable temperature CW-EPR, and pulse EPR data for a series of $[Mn^{III}Mn_3^{IV}O_4]$ cuboidal complexes. Results show that the electronic structures of tetranuclear Mn complexes are highly sensitive to even small geometric changes promoted by the nature of the supporting ligands. Similar to the computational studies performed on the S_2 state, our experimental studies on model clusters suggest that the spectroscopic properties of the OEC may also react very sensitively to small changes in structure.

RESULTS

Synthesis, crystal structure, and electrochemistry of $[Mn^{III}Mn_3^{IV}O_4]$ complexes.

One electron reduced $[Mn_2^{III}Mn_2^{IV}O_4]$ cuboidal complexes were chosen as precursors for the targeted $[Mn^{III}Mn_3^{IV}O_4]$ complexes. We have previously reported the synthesis of $LMn_2^{III}Mn_2^{IV}O_4(OAc)_3$ (**1,** Scheme 1).[56–57, 70] The cyclic voltammogram (CV) of **1** shows a reversible redox process at +250 mV vs. Fc/Fc^+ assigned to the $(Mn_2^{III}Mn_2^{IV})$/

($Mn^{III}Mn_3^{IV}$) couple. Treatment of **1** with 1 equiv. of $[(4\text{-}BrPh)_3N][SbCl_6]$ results in the formation of an unstable species, but rapid freeze-quenching of the reaction mixture allowed the observation of an intense EPR spectrum with a broad signal centered at $g = 2$ featuring Mn hyperfine interactions, consistent with an $S = 1/2$ ground state (Fig S17). In contrast, the phosphinate-bridged cuboidal complex $[Mn_4O_4(Ph_2PO_2)_6]^+$ has a higher spin ground state S ≥ 3/2. The product of oxidation of **1** features other broad EPR signals at $g > 2$ that can be assigned to spin excited states or decomposition products, but further investigation was not pursued.

Based on the reduction potential of the isolable $[Mn_4O_4(Ph_2PO_2)_6]^+$ complex at +680 mV vs. Fc/Fc^+, we targeted oxidatively stable phosphinate-bridged complexes.[41, 61] Treatment of **1** with 3 equiv. HO_2PPh_2 in THF leads to the formation of **2** via a protonolysis reaction (Scheme 1). The ESI-MS peak at m/z = 1792 is consistent with the mass of $[LMn_4O_4(O_2PPh_2)_3]^+$. The X-ray crystal structure of **2** is consistent with the $LMn_4O_4(O_2PPh_2)_3$ formulation (Fig. 2). Based on Mn−oxo distances, the oxidation states of Mn(1) and Mn(2) are assigned to Mn^{IV}, and those of Mn(3) and Mn(4) to Mn^{III}. Axial elongation of Mn^{III}−oxo distances is observed, at 2.177(2) and 2.187(2) Å for Mn(3) and Mn(4), respectively. These are due to population of a dz^2-**σ** antibonding orbital. Given the heteroleptic coordination around Mn(3), the Jahn-Teller effect is not invoked to describe the observed distortion. The coordination environment around Mn(4) can be viewed as *pseudo-*O_h, in which case the Jahn-Teller elongation can be invoked to remove the degeneracy of the ^5E_g ground state.[71–72] Similar Mn^{III}−oxo elongations were observed for **1**, at 2.201(2) and 2.234(2) Å. The CV of **2** shows a reversible redox process at +190 mV vs. Fc/Fc^+ assigned to the $(Mn_2^{III}Mn_2^{IV})/(Mn^{III}Mn_3^{IV})$ couple (Fig. 3). Treatment of **2** with 1 equiv. of $[(4\text{-}BrPh)_3N][OTf]$ leads to the formation of the one-electron oxidized species **2-ox**.[73] The ESI-MS and crystal structure of **2-ox** is consistent with the $LMn_4O_4(O_2PPh_2)_3(OTf)$ formulation (Fig. 2). Based on Mn−oxo distances, the oxidation state of Mn(4) is assigned as Mn^{III}. The elongated Mn(4)−O(4) distance of 2.241(1) Å is consistent with this assignment.

Toward expanding the series of Mn_4 clusters with the same redox state as the S_2 state of the OEC, other supporting ligands were targeted. Based on the precedent that amidate ligands have been employed for the synthesis of a high oxidation state Mn^V-oxo complex,[74] we targeted a related class of oxidatively stable amidate-bridged $[Mn_4O_4]$ cuboidal complexes. In contrast to the vast number of carboxylate-bridged high oxidation state metal-oxo clusters, amidate-bridged metal-oxo clusters are rare.[75–78] We employed an *n*-propyl-linked diacetamide proligand (H_2diam) to replace two acetate moieties. Treatment of **1** with 1 equiv. H_2diam and 2 equiv. NaO^tBu in DMF leads to the formation of **3** (Scheme 1). The ESI-MS and crystal structure of **3** are consistent with the LMn_4O_4(diam)(OAc) formulation. A smaller variation of Mn−oxo distances is observed in **3**, ranging from 1.860(2) to 2.087(2) Å. The *n*-propyl-linked diamidate serves as a bridging ligand across two faces of the $[Mn_4O_4]$ cubane moiety, resulting in a *pseudo-*C_S symmetric complex. The reversible $(Mn_2^{III}Mn_2^{IV})/(Mn^{III}Mn_3^{IV})$ couple is observed at −150 mV vs. Fc/Fc^+ (Fig. 3). The diamidate ligand decreases the oxidation potential by 400 mV relative to that of **1**. Treatment of **3** with 1 equiv. Ag(OTf) leads to the formation of the one-electron oxidized species **3-ox**. The ESI-MS and crystal structure of **3-ox** are consistent with the LMn_4O_4(diam)(OAc)(OTf)

formulation (Fig. 2). The oxidation state of Mn(3) is assigned as Mn^{III} in **3-ox**. With the exception of an elongated Mn(3)−O(3) distance of 2.051(4) Å, all other Mn−oxo distances are in the range 1.893(4)−1.937(4) Å, consistent with the $Mn^{III}Mn_3^{IV}$ oxidation state assignment.

To further investigate the effect of small geometric changes on the electronic structure of the resulting cluster, a diamidate-benzoate complex was targeted.[79] Treatment of **3** with 1 equiv. of p-$CF_3C_6H_4CO_2H$ (^{CF3}BzOH) leads to the formation of **4** via a protonolysis reaction (Scheme 1). The ESI-MS peak at m/z = 1485 is consistent with the mass of [LMn_4O_4(diam)(OBz^{CF3})]$^+$. The CV of **4** shows a reversible redox process at −15 mV vs. Fc/Fc^+ assigned to the ($Mn_2^{III}Mn_2^{IV}$)/($Mn^{III}Mn_3^{IV}$) couple (Fig. 3). The positive shift by 135 mV relative to that of **3** is consistent with the decreased basicity of OBz^- compared to OAc^-.[80–81] Treatment of **4** with 1 equiv. Ag(OTf) leads to the formation of the one-electron oxidized species **4-ox**. The LMn_4O_4(diam)(OBz)(OTf) formulation is consistent with the crystal structure (Fig. 2). Similar to **3-ox**, the oxidation state of Mn(3) is assigned as Mn^{III}. An elongated Mn(3)−O(3) distance of 2.143(3) Å is consistent with the $Mn^{III}Mn_3^{IV}$ assignment. Overall, comparing complexes **2-ox**, **3-ox**, and **4-ox**, the elongated Mn^{III}-oxo distance varies from 2.241(1), to 2.051(4), and 2.143(3), while the other Mn-oxo distances are in the range 1.831(1)−1.976(2) Å, 1.893(4)−1.937(4) Å, and 1.873(3)−1.965(3) Å, respectively. For **2-ox**, **3-ox**, and **4-ox**, the redox potential for the reversible ($Mn_2^{III}Mn_2^{IV}$)/($Mn^{III}Mn_3^{IV}$) couple was measured at +190 mV, −150 mV, and −15 mV vs. Fc/Fc^+, respectively. In comparison, the estimated midpoint redox potential for the (S_1/S_2) couple in the OEC was estimated at +900 mV vs. SHE, which is approximately +250 mV vs. Fc/Fc^+.[82]

XAS spectroscopy.

Solution and solid-state Mn K-edge X-ray absorption near-edge spectroscopy (XANES) and extended X-ray absorption fine structure (EXAFS) were used to further characterize the metal oxidation states and to provide evidence of structural integrity in solution (Fig. S12−S13). Absorption edge positions were determined from the second-derivative zero-crossings, giving the following values (eV): 6553.3 (**2-ox**), 6552.8 (**3-ox**), 6553.3 (**4-ox**). These values are comparable to 6553.1 (S_1) and 6554.1 (S_2) from cyanobacteria PSII.[20] Solution EXAFS data for **2-ox**, **3-ox**, and **4-ox** are indistinguishable from the corresponding solid-state EXAFS data and are consistent with the solid state structural assignments (Fig. 4).

Magnetometry.

To obtain insight into the magnetic exchange coupling interactions between the Mn centers, magnetic susceptibility measurements were performed on powdered crystalline samples of **2-ox**, **3-ox**, and **4-ox** in the temperature range 1.8 K−300 K at a non-saturating field of 0.4 T. For **2-ox**, the χT value of 5.64 emu K mol^{-1} at 300 K indicates antiferromagnetic coupling between the Mn centers, deviating from the expected spin-only value of 8.62 emu K mol^{-1} (g = 2) for uncoupled Mn^{III} (S = 2) and Mn^{IV} (S = 3/2) centers (Fig. 5). χT decreases monotonically with temperature, reaching a value of 0.383 emu K mol^{-1} at 1.8 K, in good agreement with the expected χT value of 0.375 emu K mol^{-1} for an S = 1/2 (g = 2) ground state. The near-ideal Curie behavior observed between 1.8−10 K can be attributed to the

absence of thermally accessible spin excited states $S > 1/2$ in this temperature range. Using software that employs an exact solution to the isotropic spin exchange Hamiltonian (Eq. 1)[83], an exchange coupling model that consists of two edge-sharing isosceles triangles with vertices at Mn(1)-Mn(2)-Mn(3) and Mn(2)-Mn(3)-Mn(4) was employed to fit the susceptibility data. This model takes into account the *pseudo*-C_S symmetry of the $[Mn_4O_4]$ core, with the mirror plane containing the Mn(4)-Mn(1) and Mn(4)-O(4) vectors and bisecting the Mn(2)-Mn(3) vector. The following parameters were used to fit the data: $J_{12} = J_{13} = -8.8$ cm^{-1}, $J_{23} = -18.7$ cm^{-1}, $J_{14} = -21.0$ cm^{-1}, $J_{24} = J_{34} = -3.2$ cm^{-1}, $g = 2.00$. The smaller $J_{24} = J_{34}$ coupling is expected given the elongated Mn(4)−O(4) distance of 2.241(1) Å. Simulating the susceptibility data assuming single-site zero field splitting parameters $D(Mn^{IV}) = 0$ cm^{-1} and $D(Mn^{III}) = 0$, −2, or −4 cm^{-1} did not result in significant differences in J. Values of $D \approx -0.2$ cm^{-1} and $D \approx -4$ cm^{-1} are typical for 6-coordinate Mn^{IV} and Mn^{III}, respectively.[17, 84–85] The calculated energy level diagram indicates a quartet excited state *c.a.* 28 cm^{-1} (equivalent temperature of 40 K) above the doublet ground state (Fig. S14). This energy separation is comparable to the 25−35 cm^{-1} measured for MeOH-treated OEC poised in the multiline S_2 state.[86]

$$\widehat{H} = -2 \sum_{i \neq j}^{i,j \in N} J_{ij} \widehat{S}_i \cdot \widehat{S}_J \quad (1)$$

Complex **3-ox** was studied by SQUID magnetometry. Similar to **2-ox**, the χT value of 5.32 emu K mol^{-1} at 300 K indicates antiferromagnetic coupling between the Mn centers (Fig. 5). χT decreases monotonically with temperature, reaching a value of 0.85 emu K mol^{-1} at 5 K. The deviation from the expected χT value of 0.38 emu K mol^{-1} ($S = 1/2$, $g = 2$) can be attributed to the presence of thermally accessible spin excited states $S > 1/2$. At 1.8 K, the χT value of 0.383 emu K mol^{-1} is in good agreement with the $S = 1/2$ ($g = 2$) ground state. To fit the susceptibility data, an isotropic exchange coupling model that consists of two edge-sharing isosceles triangles with vertices at Mn(1)-Mn(2)-Mn(3) and Mn(1)-Mn(2)-Mn(4) was employed. This model is different from that employed for **2-ox**, and takes into account the *pseudo*-C_S symmetry of the $[Mn_4O_4]$ core, with different mirror planes that contain the Mn(3)-Mn(4) and Mn(3)-O(3) vector and bisecting the Mn(1)-Mn(2) vector. The following parameters were used to fit the data: $J_{12} = -15.3$ cm^{-1}, $J_{13} = J_{23} = -8.9$ cm^{-1}, $J_{14} = J_{24} = -16.7$ cm^{-1}, $J_{34} = -10.6$ cm^{-1}, $g = 1.97$. Compared to **2-ox**, the smaller variation of exchange coupling constants is consistent with the smaller variation of Mn−oxo bond distances in **3-ox**. The calculated energy level diagram (Fig. S15) indicates the presence of a low-lying quartet excited states at 3−5 cm^{-1} (equivalent temperature of 4.3−7.2 K) above the doublet ground state. Interestingly, an energy separation of 3−6 cm^{-1} has been reported for untreated higher plant OEC in the S_2 state.[86–87]

Complex **4-ox** was studied by SQUID magnetometry. A higher χT value of 6.0 emu K mol^{-1} at 300 K indicates weaker antiferromagnetic coupling in **4-ox** compared to **3-ox**. χT decreases monotonically with temperature, reaching a value of 0.82 emu K mol^{-1} at 1.8 K, deviating significantly from the expected χT value of 0.375 emu K mol^{-1} for an $S = 1/2$ ($g = 2$) ground state. This indicates a further decreased energy separation between the ground and

excited states, as expected from the weaker antiferromagnetic coupling between the Mn centers. In fact, **4-ox** does not have a well-isolated spin ground state, *vide infra*. To fit the susceptibility data, a model identical to **3-ox** was employed. The following parameters were used to fit the data: $J_{12} = -11.6$ cm^{-1}, $J_{13} = J_{23} = -7.2$ cm^{-1}, $J_{14} = J_{24} = -11.1$ cm^{-1}, $J_{34} = -6.8$ cm^{-1}, $g = 1.97$. The calculated energy level diagram indicates that the lowest doublet and quartet states are separated by 0−1 cm^{-1} (equivalent temperature of 1.4 K) (Fig. S16). Overall, magnetic susceptibility studies indicate that the spin ladder in exchange-coupled tetranuclear Mn complexes is highly sensitive to small changes in structure and nature of the bridging ligands.

Variable-temperature X-band CW-EPR.

EPR studies were conducted in frozen solution samples of **2-ox**, **3-ox** and **4-ox**. At 5 K, the EPR spectrum of **2-ox** features a broad signal centered at $g = 2$ featuring Mn hyperfine interactions (Fig. 6). This is consistent with the $S = 1/2$ ground state determined from susceptibility studies. As the temperature is increased, the $g = 2$ signal loses intensity until no signal is observed above 15 K. Importantly, EPR signals originating from thermally populated spin excited states are not observed, in agreement with the predicted energy separation of 28 cm^{-1} (40 K) between the ground and excited states. The spectrum can be approximated by $g = [2.053, 2.003, 1.952]$, $g_{iso} = 2.00$ and the following ^{55}Mn hyperfine interactions A_i, $(A_{iso})_i$: $Mn_1 = [434, 434, 313]$, 394 MHz; $Mn_2 = [293, 155, 245]$, 231 MHz; $Mn_3 = [128, 146, 198]$, 157 MHz; $Mn_4 = [134, 133, 72]$, 113 MHz. The unique, larger Mn hyperfine coupling constant (394 MHz) is consistent with the Mn^{III} center in **2-ox**.[88] The EPR spectrum of **2-ox** is in stark contrast to that of the related $[Mn_4O_4(Ph_2PO_2)_6]^+$ complex with a higher spin ground state $S \geq 3/2$,[41] indicating that the EPR of exchange-coupled tetranuclear Mn complexes are highly sensitive to the Mn coordination environment, even if the core Mn_4O_4 cluster is maintained.

For the EPR spectrum of **3-ox** at 5 K, only the multiline signal centered at $g = 2.0$ is discernible. As the sample is warmed, the signal at $g = 2$ decreases in intensity as a signal centered at $g = 4.2$ gains intensity (Fig. 7). Above 20 K, both signals start to lose intensity due to relaxation. The signal at $g = 2$ is consistent with the $S = 1/2$ ground state determined from susceptibility studies. The $g = 4.2$ signal, assigned to the $S = 3/2$ excited state of **3-ox**, is highly reminiscent of the S_2 state in its HS form. The $g = 2$ and the $g = 4.2$ signals of the S_2 state arise from the ground states of structurally distinct species, the relative ratio of which is affected by external chemical stimuli such as pH. As such, both EPR signals can be observed at low temperatures in a ratio that reflects the relative population of the two species.[34] In the case of **3-ox**, the two signals arise from different spin states of a single, structurally static species (Fig. 4). The temperature dependence of the EPR spectrum of **3-ox** can be explained in terms of small differences in the Boltzmann distribution of the ground and excited states. At 5 K, only the $S = 1/2$ ground state is significantly populated, and the $g = 2$ signal corresponds to the $|-1/2\rangle \rightarrow |1/2\rangle$ transition. As the temperature is increased, the difference in the population of the $|-1/2\rangle$ and the $|1/2\rangle$ states decrease, resulting in weaker absorption. Concurrently, as the temperature is increased, the $S = 3/2$ spin excited state is populated, and the $g = 4.2$ signal corresponds to the transition within the $|\pm 3/2\rangle$ Kramers doublet. In contrast to **2-ox**, the observation of the $g = 4.2$ signal is consistent with a smaller

energy separation between the ground doublet and excited quartet state in **3-ox**, in agreement with the magnetic susceptibility studies. The EPR spectrum of a weakly antiferromagnetically coupled $Mn^{III}Mn^{IV}$ dimer shows a similar temperature dependence: At 20 K, only the $g = 2$ signal is observed, but upon warming to 43 K and to 110 K, a new low-field signal at $g = 5$ gains intensity.[89] This low-field signal has been assigned to the $S = 3/2$ excited state. For more strongly coupled $Mn^{III}Mn^{IV}$ dimeric systems, the quartet excited state is separated from the doublet ground state by hundreds of wavenumbers and the signal corresponding to the $S = 3/2$ excited state was not observed.[39, 90–95]

For the EPR spectrum of **4-ox**, in addition to the signal at $g = 2$, other signals assignable to $S = 3/2$ spin states were observed even at 5 K, at $g = 7.5$ and $g = 5.5$. This indicates a very small energy separation between the doublet and quartet states in **4-ox**, in agreement with the susceptibility studies. As the sample is warmed, the signal at $g = 2$ decreases in intensity. In the low field region, the $g = 7.5$ signal loses intensity upon warming, whereas the $g = 5.5$ and $g = 4.2$ signals gain intensity. At 15 K, the low-field region collapses to the $g = 4.2$ signal observed for **3-ox**. The temperature dependence of the low field region may be explained by the presence of two distinct $S = 3/2$ excited states.

^{55}Mn Davies ENDOR spectroscopy.

To gain better understanding of the Mn hyperfine interactions (HFI) in **3-ox**, ^{55}Mn Davies ENDOR spectra were collected at Q-band using the pulse sequence π-t_{RF}-π_{RF}-t_{RF}-π/2-τ-π-τ-echo. Spectra were collected at selected field positions along the electron spin-echo-detected EPR spectrum (ESE-EPR): 1170 mT, 1200 mT, 1240 mT, 1270 mT, and 1300 mT (Fig. 8a). By incorporating the ESE-EPR spectrum at D-band (130 GHz) *vide infra*, the g values were constrained to $g = [1.944, 1.964, 2.002]$, $g_{iso} = 1.97$, though it should be noted that there is no significant resolution of any individual g-values in the spectrum, likely due to slight inhomogeneity in the g-values (g-strain = 0.012 for all simulations).[96] This introduces field-dependent broadening that also causes a loss in resolution of the ^{55}Mn hyperfine structure evident in the field swept spectra as the excitation frequency is increased, a phenomenon also observed in multi-frequency EPR spectra of the S_2 state of the $CaMn_4O_5$ cluster of photosystem II.[97] A global fit of the Mn hyperfine interactions incorporating the ENDOR spectra as well as the X-band CW spectrum yields the parameters listed in Table 1. Similar to **2-ox**, the unique, larger Mn hyperfine coupling constant is consistent with the Mn^{III} center in **3-ox**.[16, 95] The Mn hyperfine coupling constants reported for **3-ox** are similar in magnitude to that of the S_2 state of *T. elongatus*.[16, 86, 97–98] Notably, ^{55}Mn ENDOR spectra for tetranuclear Mn model complexes have been hitherto absent in the literature.

ESE-EPR and electron-electron double resonance-detected NMR (EDNMR) of **3-ox** were recorded at D-band (130 GHz). EDNMR employs a high-turning angle microwave pulse which concurrently excites NMR and EPR transitions rather than an RF pulse to drive NMR transitions as in ENDOR.[99] EDNMR offers some distinctive features compared to ENDOR, including decreased selectivity between magnetic nuclei with very different gyromagnetic ratios, decreased dependence on the species of interest to exhibit long spin lattice relaxation times, and vastly enhanced signal intensity for the same amount of acquisition time.[100] However, EDNMR typically suffers from far broader lineshapes in comparison to ENDOR,

as well as combination bands and multiple-quantum transitions, which can produce complex, feature-rich spectra.[68, 101] The EDNMR spectrum of **3-ox** at $g = 1.97$ (4.7 T) is displayed in Figure S19. Features observed at 14 MHz and 200 MHz correspond to single-quantum transitions from ^{14}N and ^{1}H nuclei of the ligand scaffold (^{14}N and ^{1}H Larmor frequencies at 4.7 T are 14.4 MHz and 200 MHz, respectively). A large, broad peak is observed at 50 MHz (FWHM = 48 MHz) as well as peaks at 140 MHz, 150 MHz, and 170 MHz corresponding to ^{55}Mn single-quantum transitions. In the strong coupling limit, these couplings are centered at A/2 and split by twice the ^{55}Mn Larmor frequency (*c.a.* 50 MHz at 4.7 T). Based on the observed ^{55}Mn transitions, the ^{55}Mn HFI are estimated in the range 180–240 MHz, in line with the Mn(IV) HFI measured from Q-band ^{55}Mn ENDOR. The spectral signature of the unique Mn(III) ion cannot be unambiguously assigned from the EDNMR due to multiple overlapping transitions. Nonetheless, the general agreement of the EDNMR and ENDOR data support the hyperfine assignments of **3-ox**. The remaining features appearing from 250–350 MHz are assigned to ^{55}Mn double-quantum transitions.

The temperature dependence of electron spin-lattice relaxation in **3-ox** was studied using the inversion-recovery sequence ($\pi - t - \pi/2 - \tau - \pi -$ echo) (Fig. S18).[102] Data were fit to a bi-exponential function (Eq. 2). Subscript *f* denotes the fast relaxing process; *s* denotes the slow process. At 3.8 K, the relaxation time constants for the fast and slow exponential components were 1.3 μs and 6.3 μs, respectively. Over the temperature range studied, both $\ln(1/T_1)$ vs. $1/T$ and $\ln(1/T_1)$ vs. $\ln(T)$ are approximately linear, consistent with either an Orbach or Raman relaxation process.[86] Assuming an Orbach mechanism, an energy separation of 13 cm^{-1} was obtained from the fast relaxing component. This value is slightly larger than the 3−5 cm^{-1} estimated from susceptibility studies but approximately in the same magnitude. Overall, both electron spin-lattice relaxation and magnetic susceptibility measurements support a small separation between the doublet ground state and the quartet excited state.

$$M_z(T) = M_f\left[1 - 2\exp\left(-\frac{T}{T_{1f}}\right)\right] + M_s\left[1 - 2\exp\left(-\frac{T}{T_{1s}}\right)\right] \quad (2)$$

DISCUSSION

Between the optimized structures of the proposed open-and closed-cubane forms of the S_2 state, Mn(4)−O(5) and Mn(1)−O(5) distances interchange from 1.87 Å to ~3.2 Å, tantamount to a bond breaking-reforming process (Fig. 1). This rearrangement process is accompanied by a change in the electronic structure of the S_2 state, as explained from the computed magnetic exchange coupling constants in both open and closed forms. The $g = 2$ and the $g = 4.2$ signals of the S_2 state result from the ground states of clusters that differ significantly in geometry, the relative ratio of which is affected by external chemical stimuli. Our studies indicate that such large structural changes to the inorganic $CaMn_4O_5$ core of the OEC may not be necessary to perturb its electronic structure. Comparisons between the crystal structures of **2-ox**, **3-ox**, and **4-ox** indicate only small variations in Mn−oxo bond distances, with the longest Mn−oxo bond in each species varying from 2.051(4) Å to

2.241(1) Å. The remaining Mn-O distances are in the range 1.831(1)−1.976(2) Å. Yet, such small geometric changes in the [$Mn^{III}Mn_3^{IV}O_4$] core have a substantial effect in its electronic structure, as evident from magnetic susceptibility and EPR studies. Assigned to a thermally accessible spin excited state $S = 3/2$, the $g = 4.2$ signal in **3-ox** and **4-ox** is highly reminiscent of the S_2 state in its high-spin form. The absence of such a signal in **2-ox** indicates that spectroscopic properties of tetranuclear Mn complexes are highly dependent on the nature and magnitude of the magnetic exchange coupling interactions, which are finely tuned by the nature of not only bridging ligands but also terminal ligands in the immediate coordination sphere of each Mn ion. While the two signals observed in **3-ox** and **4-ox** are not resulting from ground states of two different isomers, as proposed in PSII, they do correspond to low-and high-spin electronic states. As in PSII, the degrees of population of the two states are affected by different coupling schemes between the Mn centers, which arise from structural differences. Most importantly, large structural distortions are not necessary for the complete disappearance of one of the signals (the HS in this case, for **2-ox**). In a previously reported $Mn^{III}Mn_3^{IV}O_4$ cubane with six phosphinate ligands, the LS signal completely disappears, consistent with a higher $S \geq 3/2$ ground state.[41] Furthermore, the energy separation between the doublet ground state and the first non-doublet excited state can be fine-tuned with small changes in the overall geometry of the cluster, as evidenced by the variable temperature EPR of **3-ox** and **4-ox** (Fig. 7). *These findings suggest that geometrical changes much smaller than the ones proposed for PSII with respect to the metal and oxo/hydroxo motifs could have substantial effects on the EPR signals. Therefore, the deduction of the geometry of OEC S-state intermediates based on EPR spectroscopic features need to be complemented with appropriate structural determination*. Given that in the present series of compounds, even a change in the nature of a single carboxylate ligand affects the state energies and EPR signals, it is expected that features such as the protonation state of aquo ligands, bridging oxos, and nearby His residues will greatly affect the electronic structure of the OEC.

In conclusion, a series of $Mn^{III}Mn_3^{IV}O_4$ cuboidal complexes has been synthesized and characterized by XRD, electrochemistry, XAS, SQUID magnetometry, variable temperature CW-EPR, and pulsed-EPR. To our knowledge this is the first set of experimental studies that directly addresses the effect of systematic changes of supporting ligands on the EPR behavior of clusters in the redox state of the S_2 state of the OEC. With implications in the interpretation of the OEC spectroscopic properties, our benchmarking results show that the electronic structure of tetranuclear Mn complexes is highly sensitive to small geometric changes and the nature of the bridging ligands. Even in the absence of large oxo movements proposed to account for the HS and LS signals of the OEC, we find that the EPR feature of essentially isostructural compounds can move from LS to a mixture of LS and HS to HS signals. Therefore, interpretation of EPR signals in terms of structural implications must be done very cautiously. Ideally, complementary structural information will be obtained to corroborate spectroscopic assignments.

Supplementary Material

Refer to Web version on PubMed Central for supplementary material.

ACKNOWLEDGMENT

This research was supported by the NIH (R01-GM102687B), the Dreyfus Teacher-Scholar Program (T.A.), Dow Next Generation Educator (instrumentation), NSF-1531940 (Caltech EPR facility), the Division of Chemical Sciences, Geosciences, and Biosciences (R.D.B. grant DE-SC0007203) of the Office of Basic Energy Sciences of the U.S. Department of Energy. Part of this work (XAS data collection) was carried out at Stanford Synchrotron Radiation Lightsource, SLAC National Accelerator Laboratory, supported by the U.S. Department of Energy, Office of Science, Office of Basic Energy Sciences under Contract No. DE-AC02–76SF00515. XAS studies were performed with support of the Office of Science, OBES, Division of Chemical Sciences, Geosciences, and Biosciences (CSGB) of the DOE under contract no. DE-AC02–05CH11231 (J.Y.). We thank Dr. Michael K. Takase and Mr. Lawrence M. Henling for assistance with X-ray crystallography; Dr. Ignacio B. Martini for SQUID magnetometry.

REFERENCES

(1). Shen J-R, The Structure of Photosystem II and the Mechanism of Water Oxidation in Photosynthesis. Annu. Rev. Plant Biol. 2015, 66, 23. [PubMed: 25746448]

(2). Yano J; Yachandra V, Mn_4Ca Cluster in Photosynthesis: Where and How Water is Oxidized to Dioxygen. Chem. Rev. 2014, 114, 4175. [PubMed: 24684576]

(3). Cox N; Pantazis DA; Neese F; Lubitz W, Biological Water Oxidation. Acc. Chem. Res. 2013, 46, 1588. [PubMed: 23506074]

(4). Oyala PH; Stich TA; Debus RJ; Britt RD, Ammonia Binds to the Dangler Manganese of the Photosystem II Oxygen-Evolving Complex. J. Am. Chem. Soc. 2015, 137, 8829. [PubMed: 26083545]

(5). Siegbahn PEM, Structures and Energetics for O_2 Formation in Photosystem II. Acc. Chem. Res. 2009, 42, 1871. [PubMed: 19856959]

(6). Oyala PH; Stich TA; Stull JA; Yu F; Pecoraro VL; Britt RD, Pulse Electron Paramagnetic Resonance Studies of the Interaction of Methanol with the S_2 State of the Mn_4O_5Ca Cluster of Photosystem II. Biochemistry 2014, 53, 7914. [PubMed: 25441091]

(7). Pérez Navarro M; Ames WM; Nilsson H; Lohmiller T; Pantazis DA; Rapatskiy L; Nowaczyk MM; Neese F; Boussac A; Messinger J; Lubitz W; Cox N, Ammonia binding to the oxygen-evolving complex of photosystem II identifies the solvent-exchangeable oxygen bridge (μ-oxo) of the manganese tetramer. Proc. Nat. Acad. Sci. 2013, 110, 15561. [PubMed: 24023065]

(8). Rapatskiy L; Cox N; Savitsky A; Ames WM; Sander J; Nowaczyk MM; Rögner M; Boussac A; Neese F; Messinger J; Lubitz W, Detection of the Water-Binding Sites of the Oxygen-Evolving Complex of Photosystem II Using W-Band ^{17}O Electron–Electron Double Resonance-Detected NMR Spectroscopy. J. Am. Chem. Soc. 2012, 134, 16619. [PubMed: 22937979]

(9). Boussac A; Rutherford AW, Comparative study of the g=4.1 EPR signals in the S_2 state of photosystem II. Biochim. Biophys. Acta 2000, 1457, 145. [PubMed: 10773159]

(10). Haddy A; Lakshmi KV; Brudvig GW; Frank HA, Q-Band EPR of the S_2 State of Photosystem II Confirms an S=5/2 Origin of the X-Band g=4.1 Signal. Biophys. J. 2004, 87, 2885. [PubMed: 15454478]

(11). Boussac A; Un S; Horner O; Rutherford AW, High-Spin States ($S \geq 5/2$) of the Photosystem II Manganese Complex. Biochemistry 1998, 37, 4001. [PubMed: 9565450]

(12). Britt RD; Lorigan GA; Sauer K; Klein MP; Zimmermann J-L, The g = 2 multiline EPR signal of the S_2 state of the photosynthetic oxygen-evolving complex originates from a ground spin state. Biochim. Biophys. Acta -Bioenergetics 1992, 1140, 95.

(13). Kim DH; Britt RD; Klein MP; Sauer K, The manganese site of the photosynthetic oxygen-evolving complex probed by EPR spectroscopy of oriented photosystem II membranes: the g = 4 and g = 2 multiline signals. Biochemistry 1992, 31, 541. [PubMed: 1310041]

(14). Dismukes GC; Siderer Y, Intermediates of a polynuclear manganese center involved in photosynthetic oxidation of water. Proc. Nat. Acad. Sci. 1981, 78, 274. [PubMed: 16592949]

(15). Krewald V; Retegan M; Cox N; Messinger J; Lubitz W; DeBeer S; Neese F; Pantazis DA, Metal oxidation states in biological water splitting. Chem. Sci. 2015, 6, 1676. [PubMed: 29308133]

(16). Peloquin JM; Campbell KA; Randall DW; Evanchik MA; Pecoraro VL; Armstrong WH; Britt RD, ^{55}Mn ENDOR of the S_2-State Multiline EPR Signal of Photosystem II: Implications on the Structure of the Tetranuclear Mn Cluster. J. Am. Chem. Soc. 2000, 122, 10926.

(17). Cox N; Retegan M; Neese F; Pantazis DA; Boussac A; Lubitz W, Electronic structure of the oxygen-evolving complex in photosystem II prior to O-O bond formation. Science 2014, 345, 804. [PubMed: 25124437]

(18). DeRose VJ; Latimer MJ; Zimmermann J-L; Mukerji I; Yachandra VK; Sauer K; Klein MP, Fluoride substitution in the Mn cluster from Photosystem II: EPR and X-ray absorption spectroscopy studies. Chem. Phys. 1995, 194, 443.

(19). Lohmiller T; Krewald V; Navarro MP; Retegan M; Rapatskiy L; Nowaczyk MM; Boussac A; Neese F; Lubitz W; Pantazis DA; Cox N, Structure, ligands and substrate coordination of the oxygen-evolving complex of photosystem II in the S_2 state: a combined EPR and DFT study. Phys. Chem. Chem. Phys. 2014, 16, 11877. [PubMed: 24525937]

(20). Glöckner C; Kern J; Broser M; Zouni A; Yachandra V; Yano J, Structural Changes of the Oxygen-evolving Complex in Photosystem II during the Catalytic Cycle. J. Biol. Chem. 2013, 288, 22607. [PubMed: 23766513]

(21). Lohmiller T; Ames W; Lubitz W; Cox N; Misra SK, EPR Spectroscopy and the Electronic Structure of the Oxygen-Evolving Complex of Photosystem II. Appl. Magn. Reson. 2013, 44, 691.

(22). Pantazis DA; Ames W; Cox N; Lubitz W; Neese F, Two Interconvertible Structures that Explain the Spectroscopic Properties of the Oxygen-Evolving Complex of Photosystem II in the S_2 State. Angew. Chem. Int. Ed. 2012, 51, 9935.

(23). Horner O; Rivière E; Blondin G; Un S; Rutherford AW; Girerd J-J; Boussac A, SQUID Magnetization Study of the Infrared-Induced Spin Transition in the S_2 State of Photosystem II: Spin Value Associated with the g = 4.1 EPR Signal. J. Am. Chem. Soc. 1998, 120, 7924.

(24). Bovi D; Narzi D; Guidoni L, The S_2 State of the Oxygen-Evolving Complex of Photosystem II Explored by QM/MM Dynamics: Spin Surfaces and Metastable States Suggest a Reaction Path Towards the S_3 State. Angew. Chem. Int. Ed. 2013, 52, 11744.

(25). Vinyard DJ; Khan S; Askerka M; Batista VS; Brudvig GW, Energetics of the S_2 State Spin Isomers of the Oxygen-Evolving Complex of Photosystem II. J. Phys. Chem. B 2017, 121, 1020. [PubMed: 28079373]

(26). Suga M; Akita F; Sugahara M; Kubo M; Nakajima Y; Nakane T; Yamashita K; Umena Y; Nakabayashi M; Yamane T; Nakano T; Suzuki M; Masuda T; Inoue S; Kimura T; Nomura T; Yonekura S; Yu L-J; Sakamoto T; Motomura T; Chen J-H; Kato Y; Noguchi T; Tono K; Joti Y; Kameshima T; Hatsui T; Nango E; Tanaka R; Naitow H; Matsuura Y; Yamashita A; Yamamoto M; Nureki O; Yabashi M; Ishikawa T; Iwata S; Shen J-R, Light-induced structural changes and the site of O=O bond formation in PSII caught by XFEL. Nature 2017, 543, 131. [PubMed: 28219079]

(27). Young ID; Ibrahim M; Chatterjee R; Gul S; Fuller FD; Koroidov S; Brewster AS; Tran R; Alonso-Mori R; Kroll T; Michels-Clark T; Laksmono H; Sierra RG; Stan CA; Hussein R; Zhang M; Douthit L; Kubin M; de Lichtenberg C; Vo Pham L; Nilsson H; Cheah MH; Shevela D; Saracini C; Bean MA; Seuffert I; Sokaras D; Weng T-C; Pastor E; Weninger C; Fransson T; Lassalle L; Bräuer P; Aller P; Docker PT; Andi B; Orville AM; Glownia JM; Nelson S; Sikorski M; Zhu D; Hunter MS; Lane TJ; Aquila A; Koglin JE; Robinson J; Liang M; Boutet S; Lyubimov AY; Uervirojnangkoorn M; Moriarty NW; Liebschner D; Afonine PV; Waterman DG; Evans G; Wernet P; Dobbek H; Weis WI; Brunger AT; Zwart PH; Adams PD; Zouni A; Messinger J; Bergmann U; Sauter NK; Kern J; Yachandra VK; Yano J, Structure of photosystem II and substrate binding at room temperature. Nature 2016, 540, 453. [PubMed: 27871088]

(28). Kern J; Tran R; Alonso-Mori R; Koroidov S; Echols N; Hattne J; Ibrahim M; Gul S; Laksmono H; Sierra RG; Gildea RJ; Han G; Hellmich J; Lassalle-Kaiser B; Chatterjee R; Brewster AS; Stan CA; Glöckner C; Lampe A; DiFiore D; Milathianaki D; Fry AR; Seibert MM; Koglin JE; Gallo E; Uhlig J; Sokaras D; Weng T-C; Zwart PH; Skinner DE; Bogan MJ; Messerschmidt M; Glatzel P; Williams GJ; Boutet S; Adams PD; Zouni A; Messinger J; Sauter NK; Bergmann U; Yano J; Yachandra VK, Taking snapshots of photosynthetic water oxidation using femtosecond X-ray diffraction and spectroscopy. Nat. Commun. 2014, 5, 4371. [PubMed: 25006873]

(29). Suga M; Akita F; Hirata K; Ueno G; Murakami H; Nakajima Y; Shimizu T; Yamashita K; Yamamoto M; Ago H; Shen J-R, Native structure of photosystem II at 1.95 Å resolution viewed by femtosecond X-ray pulses. Nature 2014, 517, 99. [PubMed: 25470056]

(30). Kern J; Alonso-Mori R; Tran R; Hattne J; Gildea RJ; Echols N; Glöckner C; Hellmich J; Laksmono H; Sierra RG; Lassalle-Kaiser B; Koroidov S; Lampe A; Han G; Gul S; DiFiore D; Milathianaki D; Fry AR; Miahnahri A; Schafer DW; Messerschmidt M; Seibert MM; Koglin JE; Sokaras D; Weng T-C; Sellberg J; Latimer MJ; Grosse-Kunstleve RW; Zwart PH; White WE; Glatzel P; Adams PD; Bogan MJ; Williams GJ; Boutet S; Messinger J; Zouni A; Sauter NK; Yachandra VK; Bergmann U; Yano J, Simultaneous Femtosecond X-ray Spectroscopy and Diffraction of Photosystem II at Room Temperature. Science 2013, 340, 491. [PubMed: 23413188]

(31). Kupitz C; Basu S; Grotjohann I; Fromme R; Zatsepin NA; Rendek KN; Hunter MS; Shoeman RL; White TA; Wang D; James D; Yang J-H; Cobb DE; Reeder B; Sierra RG; Liu H; Barty A; Aquila AL; Deponte D; Kirian RA; Bari S; Bergkamp JJ; Beyerlein KR; Bogan MJ; Caleman C; Chao T-C; Conrad CE; Davis KM; Fleckenstein H; Galli L; Hau-Riege SP; Kassemeyer S; Laksmono H; Liang M; Lomb L; Marchesini S; Martin AV; Messerschmidt M; Milathianaki D; Nass K; Ros A; Roy-Chowdhury S; Schmidt K; Seibert M; Steinbrener J; Stellato F; Yan L; Yoon C; Moore TA; Moore AL; Pushkar Y; Williams GJ; Boutet S; Doak RB; Weierstall U; Frank M; Chapman HN; Spence JCH; Fromme P, Serial time-resolved crystallography of photosystem II using a femtosecond X-ray laser. Nature 2014, 513, 261. [PubMed: 25043005]

(32). Sauter NK; Echols N; Adams PD; Zwart PH; Kern J; Brewster AS; Koroidov S; Alonso-Mori R; Zouni A; Messinger J; Bergmann U; Yano J; Yachandra VK, No observable conformational changes in PSII. Nature 2016, 533, E1. [PubMed: 27193689]

(33). Boussac A; Rutherford AW; Sugiura M, Electron transfer pathways from the S_2-states to the S_3-states either after a Ca^{2+}/Sr^{2+} or a Cl^{-}/I^{-} exchange in Photosystem II from Thermosynechococcus elongatus. Biochim. Biophys. Acta -Bioenergetics 2015, 1847, 576.

(34). Boussac A; Ugur I; Marion A; Sugiura M; Kaila VRI; Rutherford AW, The low spin -high spin equilibrium in the S_2-state of the water oxidizing enzyme. Biochim. Biophys. Acta - Bioenergetics 2018, 1859, 342. [PubMed: 29499187]

(35). Ames W; Pantazis DA; Krewald V; Cox N; Messinger J; Lubitz W; Neese F, Theoretical Evaluation of Structural Models of the S_2 State in the Oxygen Evolving Complex of Photosystem II: Protonation States and Magnetic Interactions. J. Am. Chem. Soc. 2011, 133, 19743. [PubMed: 22092013]

(36). Liang W; Latimer MJ; Dau H; Roelofs TA; Yachandra VK; Sauer K; Klein MP, Correlation between Structure and Magnetic Spin State of the Manganese Cluster in the Oxygen-Evolving Complex of Photosystem II in the S_2 State: Determination by X-ray Absorption Spectroscopy. Biochemistry 1994, 33, 4923. [PubMed: 8161553]

(37). Chatterjee R; Han G; Kern J; Gul S; Fuller FD; Garachtchenko A; Young ID; Weng T-C; Nordlund D; Alonso-Mori R; Bergmann U; Sokaras D; Hatakeyama M; Yachandra VK; Yano J, Structural changes correlated with magnetic spin state isomorphism in the S2 state of the Mn4CaO5 cluster in the oxygen-evolving complex of photosystem II. Chem. Sci. 2016, 7, 5236. [PubMed: 28044099]

(38). Paul S; Neese F; Pantazis DA, Structural models of the biological oxygen-evolving complex: achievements, insights, and challenges for biomimicry. Green Chem. 2017, 19, 2309.

(39). Mukhopadhyay S; Mandal SK; Bhaduri S; Armstrong WH, Manganese Clusters with Relevance to Photosystem II. Chem. Rev. 2004, 104, 3981. [PubMed: 15352784]

(40). Mullins CS; Pecoraro VL, Reflections on small molecule manganese models that seek to mimic photosynthetic water oxidation chemistry. Coord. Chem. Rev. 2008, 252, 416. [PubMed: 19081816]

(41). Ruettinger WF; Ho DM; Dismukes GC, Protonation and Dehydration Reactions of the $Mn_4O_4L_6$ Cubane and Synthesis and Crystal Structure of the Oxidized Cubane $[Mn_4O_4L_6]^{+}$: A Model for the Photosynthetic Water Oxidizing Complex. Inorg. Chem. 1999, 38, 1036. [PubMed: 11670881]

(42). Dubé CE; Sessoli R; Hendrich MP; Gatteschi D; Armstrong WH, A Spin Topological Model for the g = 4.1 S_2 State Photosystem II Water Oxidase Manganese Aggregate. J. Am. Chem. Soc. 1999, 121, 3537.

(43). Blondin G; Davydov R; Philouze C; Charlot M-F; Styring S; Akermark B; Girerd J-J; Boussac A, Electron paramagnetic resonance study of the S=1/2 ground state of a radiolysis-generated manganese(III)-trimanganese(IV) form of [MnIV4O6(bipy)6]4+ (bipy=2,2'-bipyridine). Comparison with the photosynthetic Oxygen Evolving Complex. J. Chem. Soc., Dalton Trans. 1997, 4069.

(44). Zhang C; Chen C; Dong H; Shen J-R; Dau H; Zhao J, A synthetic Mn4Ca-cluster mimicking the oxygen-evolving center of photosynthesis. Science 2015, 348, 690. [PubMed: 25954008]

(45). Shoji M; Isobe H; Shen J-R; Yamaguchi K, Geometric and electronic structures of the synthetic Mn_4CaO_4 model compound mimicking the photosynthetic oxygen-evolving complex. Phys. Chem. Chem. Phys. 2016, 18, 11330. [PubMed: 27055567]

(46). Paul S; Cox N; Pantazis DA, What Can We Learn from a Biomimetic Model of Nature's Oxygen-Evolving Complex? Inorg. Chem. 2017, 56, 3875. [PubMed: 28291351]

(47). Dubé CE; Mukhopadhyay S; Bonitatebus PJ; Staples RJ; Armstrong WH, Tuning Tetranuclear Manganese−Oxo Core Electronic Properties: Adamantane-Shaped Complexes Synthesized by Ligand Exchange. Inorg. Chem. 2005, 44, 5161. [PubMed: 15998046]

(48). Krewald V; Neese F; Pantazis DA, On the Magnetic and Spectroscopic Properties of High-Valent Mn_3CaO_4 Cubanes as Structural Units of Natural and Artificial Water-Oxidizing Catalysts. J. Am. Chem. Soc. 2013, 135, 5726. [PubMed: 23527603]

(49). Mukherjee S; Stull JA; Yano J; Stamatatos TC; Pringouri K; Stich TA; Abboud KA; Britt RD; Yachandra VK; Christou G, Synthetic model of the asymmetric [Mn_3CaO_4] cubane core of the oxygen-evolving complex of photosystem II. Proc. Nat. Acad. Sci. 2012, 109, 2257. [PubMed: 22308383]

(50). Hendrickson DN; Christou G; Schmitt EA; Libby E; Bashkin JS; Wang S; Tsai HL; Vincent JB; Boyd PDW, Photosynthetic water oxidation center: spin frustration in distorted cubane $Mn^{IV}Mn^{III3}$ model complexes. J. Am. Chem. Soc. 1992, 114, 2455.

(51). Hewitt IJ; Tang J-K; Madhu NT; Clérac R; Buth G; Anson CE; Powell AK, A series of new structural models for the OEC in photosystem II. Chem. Commun. 2006, 2650.

(52). Koumousi ES; Mukherjee S; Beavers CM; Teat SJ; Christou G; Stamatatos TC, Towards models of the oxygen-evolving complex (OEC) of photosystem II: a Mn4Ca cluster of relevance to low oxidation states of the OEC. Chem. Commun. 2011, 47, 11128.

(53). Tsui EY; Tran R; Yano J; Agapie T, Redox-inactive metals modulate the reduction potential in heterometallic manganese–oxido clusters. Nat. Chem. 2013, 5, 293. [PubMed: 23511417]

(54). Tsui EY; Agapie T, Reduction potentials of heterometallic manganese–oxido cubane complexes modulated by redox-inactive metals. Proc. Nat. Acad. Sci. 2013, 110, 10084. [PubMed: 23744039]

(55). Kanady JS; Tran R; Stull JA; Lu L; Stich TA; Day MW; Yano J; Britt RD; Agapie T, Role of oxido incorporation and ligand lability in expanding redox accessibility of structurally related Mn4 clusters. Chem. Sci. 2013, 4, 3986. [PubMed: 24163730]

(56). Kanady JS; Lin P-H; Carsch KM; Nielsen RJ; Takase MK; Goddard WA; Agapie T, Toward Models for the Full Oxygen-Evolving Complex of Photosystem II by Ligand Coordination To Lower the Symmetry of the Mn_3CaO_4 Cubane: Demonstration That Electronic Effects Facilitate Binding of a Fifth Metal. J. Am. Chem. Soc. 2014, 136, 14373. [PubMed: 25241826]

(57). Kanady JS; Mendoza-Cortes JL; Tsui EY; Nielsen RJ; Goddard WA; Agapie T, Oxygen Atom Transfer and Oxidative Water Incorporation in Cuboidal Mn_3MO_n Complexes Based on Synthetic, Isotopic Labeling, and Computational Studies. J. Am. Chem. Soc. 2013, 135, 1073. [PubMed: 23241061]

(58). Lin P-H; Tsui EY; Habib F; Murugesu M; Agapie T, Effect of the Mn Oxidation State on Single-Molecule-Magnet Properties: MnIII vs MnIV in Biologically Inspired DyMn3O4 Cubanes. Inorg. Chem. 2016, 55, 6095. [PubMed: 27281290]

(59). Han Z; Horak KT; Lee HB; Agapie T, Tetranuclear Manganese Models of the OEC Displaying Hydrogen Bonding Interactions: Application to Electrocatalytic Water Oxidation to Hydrogen Peroxide. J. Am. Chem. Soc. 2017, 139, 9108. [PubMed: 28587453]

(60). Lee HB; Tsui EY; Agapie T, A $CaMn_4O_2$ model of the biological oxygen evolving complex: synthesis via cluster expansion on a low symmetry ligand. Chem. Commun. 2017, 53, 6832.

(61). Ruettinger WF; Campana C; Dismukes GC, Synthesis and Characterization of $Mn_4O_4L_6$ Complexes with Cubane-like Core Structure: A New Class of Models of the Active Site of the Photosynthetic Water Oxidase. J. Am. Chem. Soc. 1997, 119, 6670.

(62). Limburg J; Vrettos JS; Liable-Sands LM; Rheingold AL; Crabtree RH; Brudvig GW, A Functional Model for O-O Bond Formation by the O2-Evolving Complex in Photosystem II. Science 1999, 283, 1524. [PubMed: 10066173]

(63). Limburg J; Vrettos JS; Chen H; de Paula JC; Crabtree RH; Brudvig GW, Characterization of the O2-Evolving Reaction Catalyzed by [(terpy)(H2O)MnIII(O)2MnIV(OH2)(terpy)](NO3)3 (terpy = 2,2':6,2' '-Terpyridine). J. Am. Chem. Soc. 2001, 123, 423. [PubMed: 11456544]

(64). Chen H; Faller JW; Crabtree RH; Brudvig GW, Dimer-of-Dimers Model for the Oxygen-Evolving Complex of Photosystem II. Synthesis and Properties of [MnIV4O5(terpy)4(H2O)2](ClO4)6. J. Am. Chem. Soc. 2004, 126, 7345. [PubMed: 15186173]

(65). Chen;Collomb M-N; Duboc C; Blondin G; Rivière E; Faller JW; Crabtree RH; Brudvig GW, New Linear High-Valent Tetranuclear Manganese-Oxo Cluster Relevant to the Oxygen-Evolving Complex of Photosystem II with Oxo, Hydroxo, and Aqua Coordinated to a Single Mn(IV). Inorg. Chem. 2005, 44, 9567. [PubMed: 16323946]

(66). Dubé CE; Wright DW; Pal S; Bonitatebus PJ; Armstrong WH, Tetranuclear Manganese-Oxo Aggregates Relevant to the Photosynthetic Water Oxidation Center. Crystal Structure, Spectroscopic Properties and Reactivity of Adamantane-Shaped [Mn4O6(bpea)4]4+ and the Reduced Mixed-Valence Analog [Mn4O6(bpea)4]3+. J. Am. Chem. Soc. 1998, 120, 3704.

(67). Chan MK; Armstrong WH, Tetranuclear manganese-oxo complex with a 2.7 A Mn-Mn separation and intramolecular H2O-(mu-O) hydrogen-bonded contacts: [Mn4O2(TPHPN)2(H2O)2(CF3SO3)2](CF3SO3)3. Possible mode for binding of water at the active site of the oxygen-evolving complex in photosystem II. J. Am. Chem. Soc. 1990, 112, 4985.

(68). Nguyen AI; Suess DLM; Darago LE; Oyala PH; Levine DS; Ziegler MS; Britt RD; Tilley TD, Manganese–Cobalt Oxido Cubanes Relevant to Manganese-Doped Water Oxidation Catalysts. J. Am. Chem. Soc. 2017, 139, 5579. [PubMed: 28347135]

(69). Nguyen AI; Darago LE; Balcells D; Tilley TD, Influence of a "Dangling" Co(II) Ion Bound to a [MnCo3O4] Oxo Cubane. J. Am. Chem. Soc. 2018, 140, 9030. [PubMed: 30001620]

(70). Kanady JS; Tsui EY; Day MW; Agapie T, A Synthetic Model of the Mn3Ca Subsite of the Oxygen-Evolving Complex in Photosystem II. Science 2011, 333, 733. [PubMed: 21817047]

(71). Carver G; Thut M; Noble C; Tregenna-Piggott PLW, Theory of High-Spin d4 Complexes: An Angular-Overlap Model Parametrization of the Ligand Field in Vibronic-Coupling Calculations. J. Chem. Theory Comput. 2008, 4, 603. [PubMed: 26620935]

(72). Tregenna-Piggott PLW; Weihe H; Barra A-L, High-Field, Multifrequency EPR Study of the [Mn(OH2)6]3+ Cation: Influence of π-Bonding on the Ground State Zero-Field-Splitting Parameters. Inorg. Chem. 2003, 42, 8504. [PubMed: 14658906]

(73). Reed CJ; Agapie T, Tetranuclear Fe Clusters with a Varied Interstitial Ligand: Effects on the Structure, Redox Properties, and Nitric Oxide Activation. Inorg. Chem. 2017, 56, 13360. [PubMed: 29052979]

(74). Gupta R; Taguchi T; Lassalle-Kaiser B; Bominaar EL; Yano J; Hendrich MP; Borovik AS, High-Spin Mn–Oxo Complexes and Their Relevance to the Oxygen-Evolving Complex Within Photosystem II. Proc. Nat. Acad. Sci. 2015, 112, 5319. [PubMed: 25852147]

(75). Tsui EY; Kanady JS; Agapie T, Synthetic Cluster Models of Biological and Heterogeneous Manganese Catalysts for O2 Evolution. Inorg. Chem. 2013, 52, 13833. [PubMed: 24328344]

(76). Christou G, Manganese carboxylate chemistry and its biological relevance. Acc. Chem. Res. 1989, 22, 328.

(77). Thomson RK; Patrick BO; Schafer LL, Synthesis, characterization, and reactivity of the first hafnium alkyl complex stabilized by amidate ligands. Can. J. Chem. 2005, 83, 1037.

(78). Xu J-Y; Astner J; Walter O; Heinemann FW; Schindler S; Merkel M; Krebs B, Iron(III) Complexes with the Ligand N′,N′-Bis[(2-pyridyl)methyl]ethylenediamine (uns-penp) and Its Amide Derivative N-Acetyl-N′,N′-bis[(2-pyridyl)methyl]ethylenediamine (acetyl-uns-penp). Eur. J. Inorg. Chem. 2006, 2006, 1601.

(79). Kampert E; Janssen FFBJ; Boukhvalov DW; Russcher JC; Smits JMM; de Gelder R; de Bruin B; Christianen PCM; Zeitler U; Katsnelson MI; Maan JC; Rowan AE, Ligand-Controlled Magnetic Interactions in Mn4 Clusters. Inorg. Chem. 2009, 48, 11903. [PubMed: 19916527]

(80). Kütt A; Leito I; Kaljurand I; Sooväli L; Vlasov VM; Yagupolskii LM; Koppel IA, A Comprehensive Self-Consistent Spectrophotometric Acidity Scale of Neutral Brønsted Acids in Acetonitrile. J. Org. Chem. 2006, 71, 2829. [PubMed: 16555839]

(81). Nguyen AI; Wang J; Levine DS; Ziegler MS; Tilley TD, Synthetic control and empirical prediction of redox potentials for Co4O4 cubanes over a 1.4 V range: implications for catalyst design and evaluation of high-valent intermediates in water oxidation. Chem. Sci. 2017, 8, 4274. [PubMed: 29081963]

(82). Rappaport F; Guergova-Kuras M; Nixon PJ; Diner BA; Lavergne J, Kinetics and Pathways of Charge Recombination in Photosystem II. Biochemistry 2002, 41, 8518. [PubMed: 12081503]

(83). Chilton NF; Anderson RP; Turner LD; Soncini A; Murray KS, PHI: A powerful new program for the analysis of anisotropic monomeric and exchange-coupled polynuclear d-and f-block complexes. J. Comput. Chem. 2013, 34, 1164. [PubMed: 23386394]

(84). Krzystek J; Ozarowski A; Telser J, Multi-frequency, high-field EPR as a powerful tool to accurately determine zero-field splitting in high-spin transition metal coordination complexes. Coord. Chem. Rev. 2006, 250, 2308.

(85). Telser J; Ozarowski A; Krzystek J, High-frequency and -field electron paramagnetic resonance of transition metal ion (d block) coordination complexes. In Electron Paramagnetic Resonance: Volume 23, The Royal Society of Chemistry: 2013; Vol. 23, pp 209.

(86). Su J-H; Cox N; Ames W; Pantazis DA; Rapatskiy L; Lohmiller T; Kulik LV; Dorlet P; Rutherford AW; Neese F; Boussac A; Lubitz W; Messinger J, The electronic structures of the S_2 states of the oxygen-evolving complexes of photosystem II in plants and cyanobacteria in the presence and absence of methanol. Biochim. Biophys. Acta -Bioenergetics 2011, 1807, 829.

(87). Pace RJ; Smith P; Bramley R; Stehlik D, EPR saturation and temperature dependence studies on signals from the oxygen-evolving centre of photosystem II. Biochim. Biophys. Acta - Bioenergetics 1991, 1058, 161.

(88). Randall DW; Sturgeon BE; Ball JA; Lorigan GA; Chan MK; Klein MP; Armstrong WH; Britt RD, 55Mn ESE-ENDOR of a Mixed Valence Mn(III)Mn(IV) Complex: Comparison with the Mn Cluster of the Photosynthetic Oxygen-Evolving Complex. J. Am. Chem. Soc. 1995, 117, 11780.

(89). Larson E; Haddy A; Kirk ML; Sands RH; Hatfield WE; Pecoraro VL, Asymmetric mixed-valent complex {[Mn(2-OH-3,5-Cl2-SALPN)]2(THF)}ClO4 shows a temperature-dependent interconversion between g = 2 multiline and low-field EPR signals. J. Am. Chem. Soc. 1992, 114, 6263.

(90). Hagen KS; Armstrong WH; Hope H, Isolation of a bis-oxo-bridged manganese(III)manganese(IV) intermediate by regulated air oxidation. Synthesis, structure, and properties of dioxobis[tris(aminoethyl)amine]dimanganese(5+) trifluoromethylsulfonate. Inorg. Chem. 1988, 27, 967.

(91). Brewer KJ; Calvin M; Lumpkin RS; Otvos JW; Spreer LO, Synthesis, structure, and characterization of a mixed-valence manganese(III)-manganese(IV) bis(mu-oxo) complex with a macrocyclic tetraaza ligand. Inorg. Chem. 1989, 28, 4446.

(92). Pal S; Gohdes JW; Wilisch WCA; Armstrong WH, Synthesis, structure, and properties of a complex that consists of an {Mn2O2(O2CCH3)}2+ core and a spanning hexadentate ligand. Inorg. Chem. 1992, 31, 713.

(93). Bashkin JS; Schake AR; Vincent JB; Chang HR; Li Q; Huffman JC; Christou G; Hendrickson DN, Mixed valence manganese-(II, III) and -(III, IV) dinuclear complexes: preparation, structure, magnetochemistry, and e.s.r. spectra of Mn2(biphen)2(biphenH)(bpy)2 and Mn2O2Cl2(OAc)

(bpy)2(biphenH2= 2,2′-biphenol, bpy = 2,2′-bipyridine). J. Chem. Soc., Chem. Commun. 1988, 700.

(94). Wieghardt K; Bossek U; Zsolnai L; Huttner G; Blondin G; Girerd J-J; Babonneau F, A novel mixed-valent Mn–Mn-dimer, [L2Mn2(μ-O)2(μ-MeCO2)][BPh4]2·MeCN: crystal structure, magnetic properties, and e.s.r. spectrum (L = 1,4,7-triazacyclononane). J. Chem. Soc., Chem. Commun. 1987, 651.

(95). Schäfer K-O; Bittl R; Zweygart W; Lendzian F; Haselhorst G; Weyhermüller T; Wieghardt K; Lubitz W, Electronic Structure of Antiferromagnetically Coupled Dinuclear Manganese (MnIIIMnIV) Complexes Studied by Magnetic Resonance Techniques. J. Am. Chem. Soc. 1998, 120, 13104.

(96). Stoll S; Schweiger A, EasySpin, a comprehensive software package for spectral simulation and analysis in EPR. J. Magn. Reson. 2006, 178, 42. [PubMed: 16188474]

(97). Cox N; Rapatskiy L; Su J-H; Pantazis DA; Sugiura M; Kulik L; Dorlet P; Rutherford AW; Neese F; Boussac A; Lubitz W; Messinger J, Effect of Ca^{2+}/Sr^{2+} Substitution on the Electronic Structure of the Oxygen-Evolving Complex of Photosystem II: A Combined Multifrequency EPR, ^{55}Mn-ENDOR, and DFT Study of the S_2 State. J. Am. Chem. Soc. 2011, 133, 3635. [PubMed: 21341708]

(98). Kulik LV; Epel B; Lubitz W; Messinger J, Electronic Structure of the Mn_4O_xCa Cluster in the S_0 and S_2 States of the Oxygen-Evolving Complex of Photosystem II Based on Pulse ^{55}Mn-ENDOR and EPR Spectroscopy. J. Am. Chem. Soc. 2007, 129, 13421. [PubMed: 17927172]

(99). Schosseler P; Wacker T; Schweiger A, Pulsed ELDOR detected NMR. Chem. Phys. Lett. 1994, 224, 319.

(100). Cox N; Lubitz W; Savitsky A, W-band ELDOR-detected NMR (EDNMR) spectroscopy as a versatile technique for the characterisation of transition metal–ligand interactions. Mol. Phys. 2013, 111, 2788.

(101). Cox N; Nalepa A; Lubitz W; Savitsky A, ELDOR-detected NMR: A general and robust method for electron-nuclear hyperfine spectroscopy? J. Magn. Reson. 2017, 280, 63. [PubMed: 28579103]

(102). Lorigan GA; Britt RD, Electron spin-lattice relaxation studies of different forms of the S_2 state multiline EPR signal of the Photosystem II oxygen-evolving complex. Photosynth. Res. 2000, 66, 189. [PubMed: 16228419]

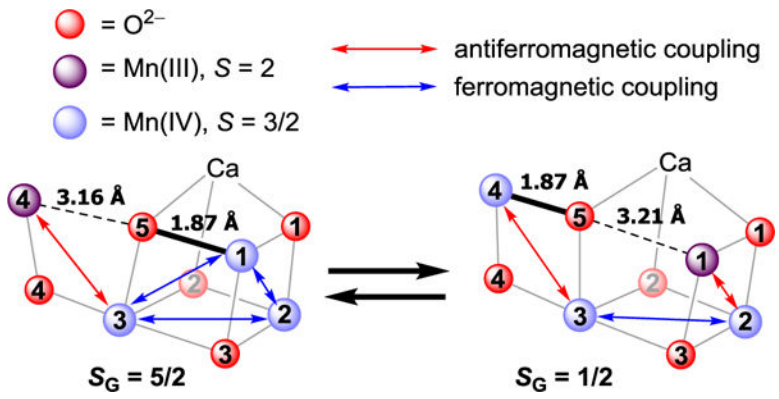

Figure 1.

Computed structures for the proposed isomers of the inorganic $CaMn_4O_5$ core of the OEC in the S_2 state. The large structural changes in the Mn-oxo distances have been calculated to lead to different electronic coupling between the Mn centers and a change in the spin ground state (S_G), which explain the two observed EPR signals. Mn(4)−O(5) and Mn(1)−O(5) distances shown with bold and dashed lines. Nature of the computed magnetic exchange coupling interactions shown in red (antiferromagnetic) and blue (ferromagnetic) arrows. Adapted from ref. 22.

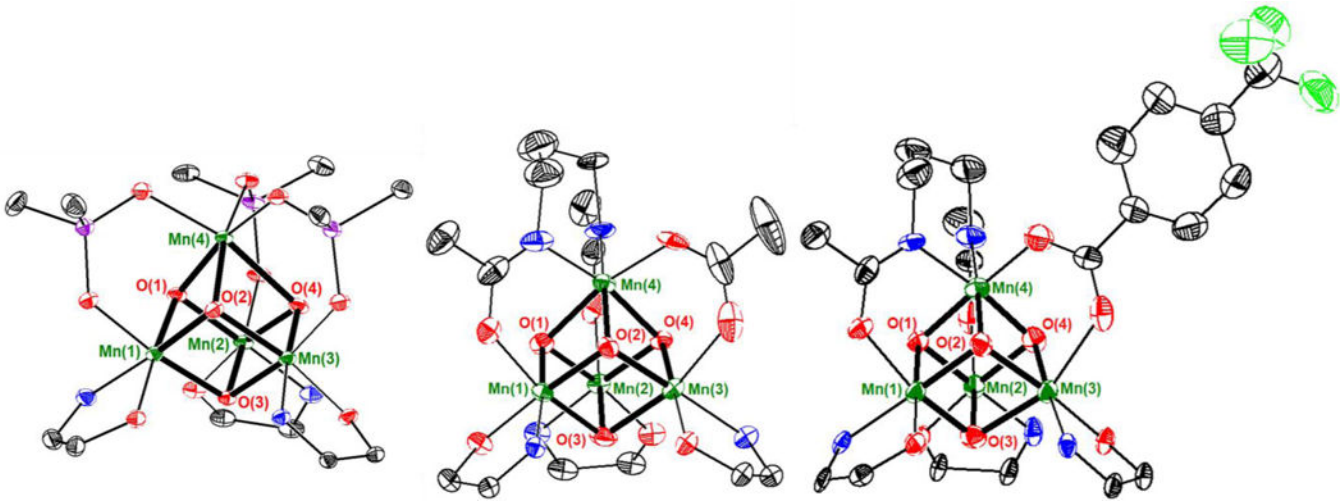

Figure 2.

Truncated crystal structures of **2-ox** (left), **3-ox** (middle), and **4-ox** (right). Mn (green), O (red), N (blue), P (purple), C (black), F (light green). Bolded bonds highlight metal-oxo bonds. Selected bond distances (Å):

2-ox: Mn(1)−O(1) 1.920(1), Mn(1)−O(2) 1.862(1), Mn(1)−O(3) 1.919(1), Mn(2)−O(1) 1.898(1), Mn(2)−O(3) 1.920(1), Mn(2)−O(4) 1.858(1), Mn(3)−O(2) 1.931(1), Mn(3)−O(3) 1.929(1), Mn(3)−O(4) 1.831(1), Mn(4)−O(1) 1.932(1), Mn(4)−O(2) 1.976(2), Mn(4)−O(4) 2.241(1), Mn(1)−Mn(2) 2.8862(8), Mn(1)−Mn(3) 2.8803(7), Mn(2)−Mn(3) 2.8477(5), Mn(1)−Mn(4) 2.8512(6), Mn(2)−Mn(4) 2.9288(6), Mn(3)−Mn(4) 2.9585(7).

3-ox: Mn(1)−O(1) 1.909(5), Mn(1)−O(2) 1.896(3), Mn(1)−O(3) 1.937(4), Mn(2)−O(1) 1.893(4), Mn(2)−O(3) 1.931(5), Mn(2)−O(4) 1.899(3), Mn(3)−O(2) 1.911(4), Mn(3)−O(3) 2.051(4), Mn(3)−O(4) 1.926(4), Mn(4)−O(1) 1.897(4), Mn(4)−O(2) 1.909(4), Mn(4)−O(4) 1.901(4), Mn(1)−Mn(2) 2.899(2), Mn(1)−Mn(3) 2.946(1), Mn(2)−Mn(3) 2.962(1), Mn(1)−Mn(4) 2.777(1), Mn(2)−Mn(4) 2.758(1), Mn(3)−Mn(4) 2.804(1).

4-ox: Mn(1)−O(1) 1.901(2), Mn(1)−O(2) 1.873(3), Mn(1)−O(3) 1.874(3), Mn(2)−O(1) 1.880(3), Mn(2)−O(3) 1.892(3), Mn(2)−O(4) 1.902(3), Mn(3)−O(2) 1.926(3), Mn(3)−O(3) 2.143(3), Mn(3)−O(4) 1.965(3), Mn(4)−O(1) 1.894(3), Mn(4)−O(2) 1.917(3), Mn(4)−O(4) 1.883(3), Mn(1)−Mn(2) 2.8725(6), Mn(1)−Mn(3) 2.9352(9), Mn(2)−Mn(3) 2.989(1), Mn(1)−Mn(4) 2.7593(7), Mn(2)−Mn(4) 2.7464(8), Mn(3)−Mn(4) 2.840(1).

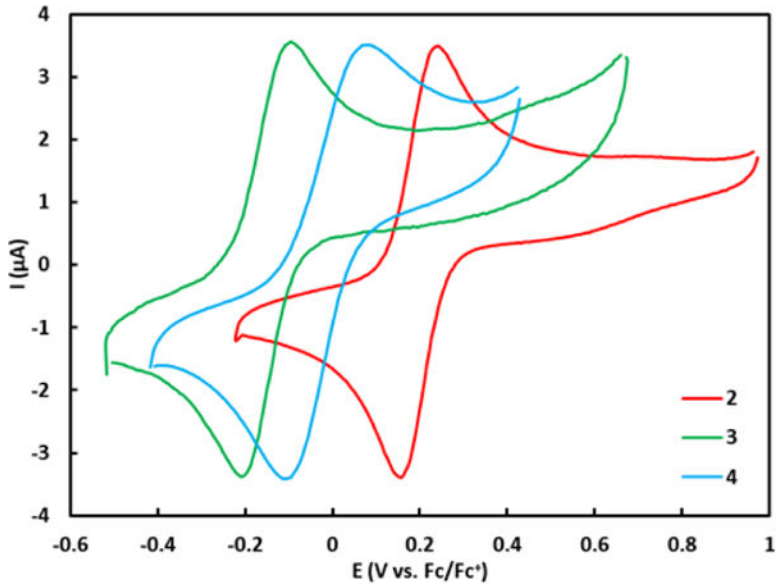

Figure 3.

CV of complexes **2**, **3**, and **4**. Measured $E_{1/2}$: −150 mV (**3**), −15 mV (**4**), +190 mV (**2**) vs. Fc/Fc^+. Estimated $E_{1/2}(S_1/S_2)$: +250 mV vs. Fc/Fc^+ (ref. 29).

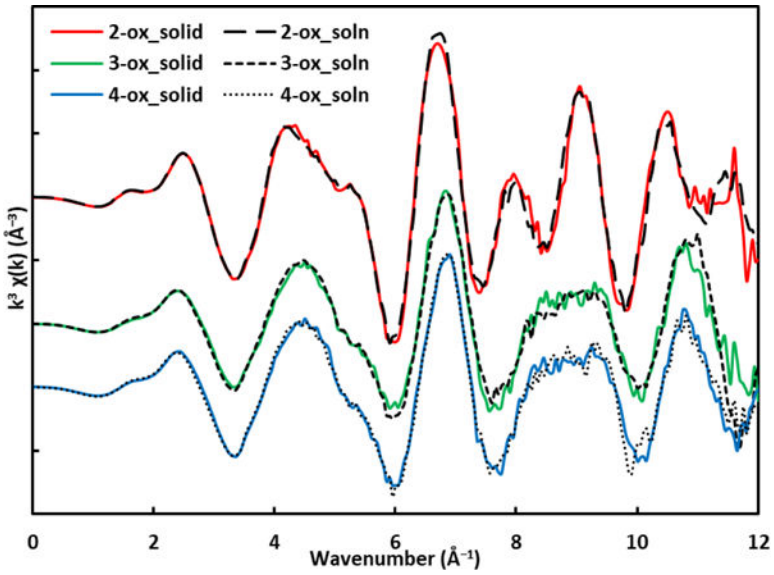

Figure 4.

k^3-weighted k-space EXAFS data at Mn K-edge for complexes **2-ox**, **3-ox**, and **4-ox** in solid and solution phases highlighting the integrity of the complexes in solution.

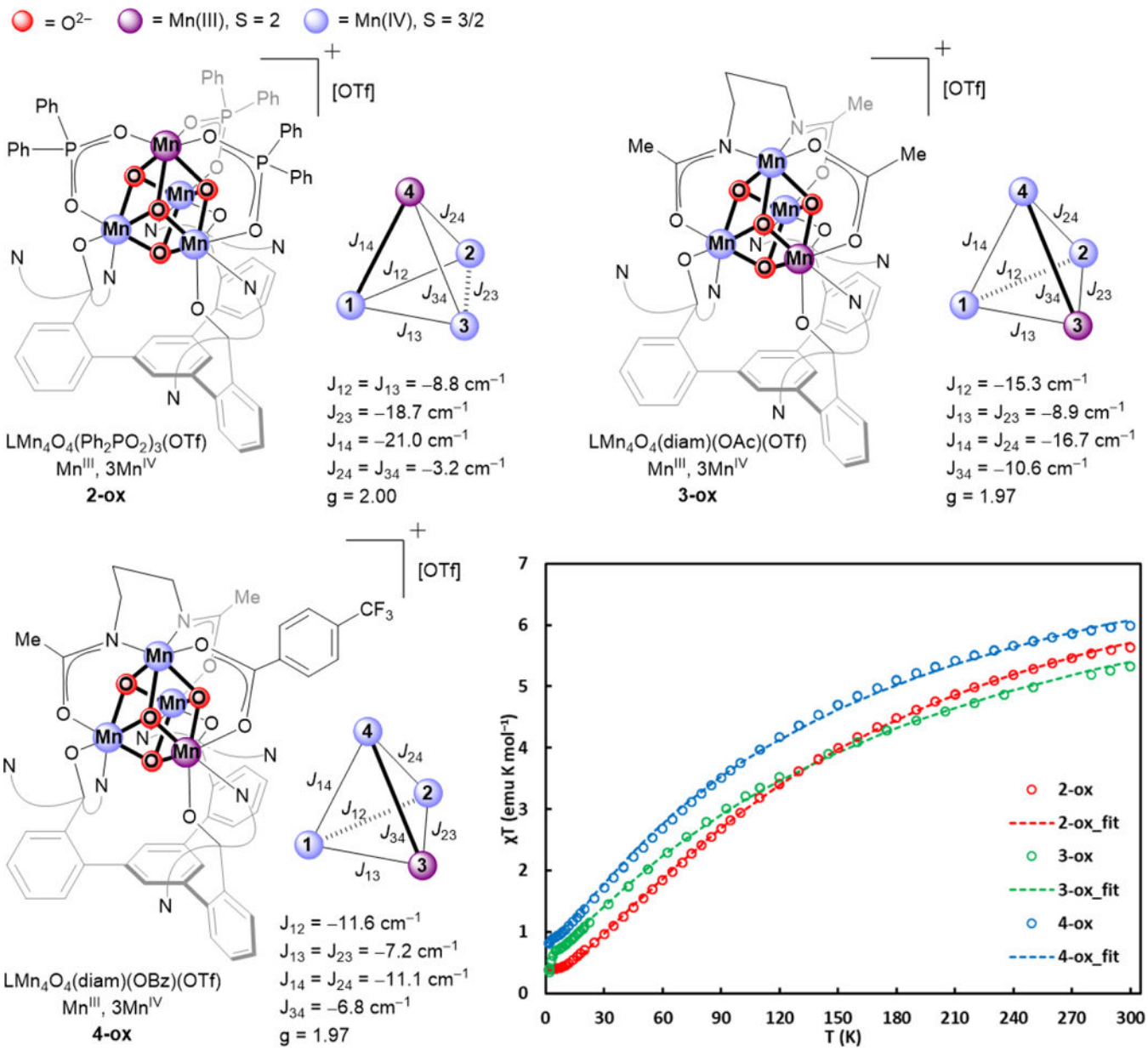

Figure 5.

Exchange coupling model, fit parameters, and χT vs. T plot of complexes **2-ox**, **3-ox**, and **4-ox**. For the exchange coupling models, the mirror plane of the *pseudo*-C_S symmetry contains the bold vector and bisects the hashed vector.

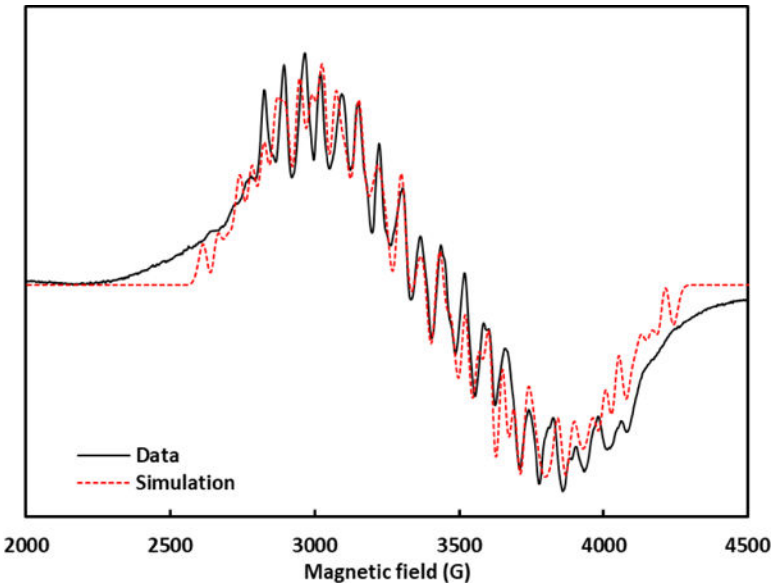

Figure 6.

X-band EPR spectrum of **2-ox**. Acquisition parameters: frequency = 9.64 MHz, power = 8 mW, conversion time = 20.48 ms, modulation amplitude = 8 G. See text for simulation parameters.

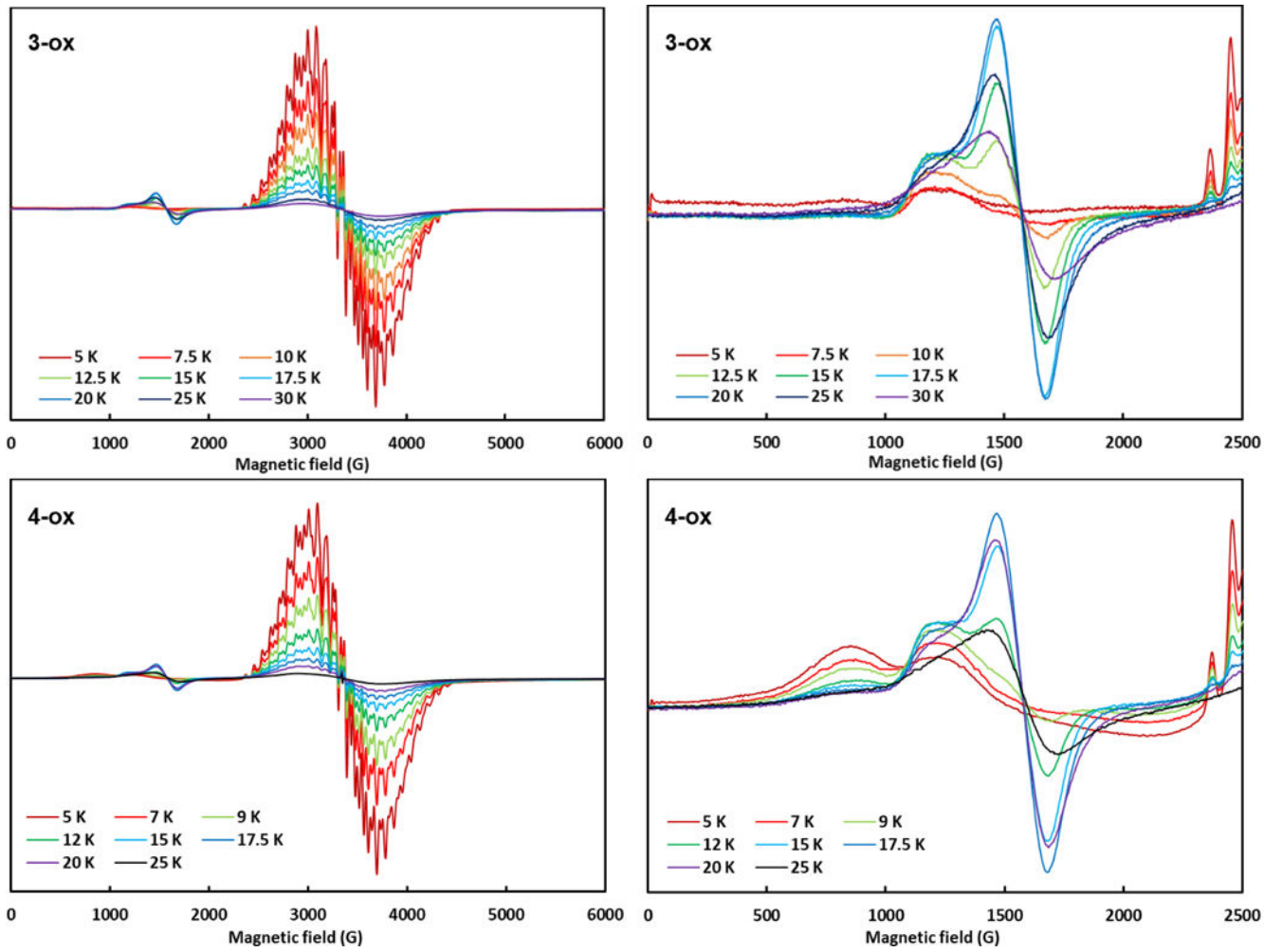

Figure 7.

(Left) Variable-temperature X-band continuous-wave EPR spectra of **3-ox** and **4-ox**. (Right) Expanded view of the low field ($g > 2$) region.

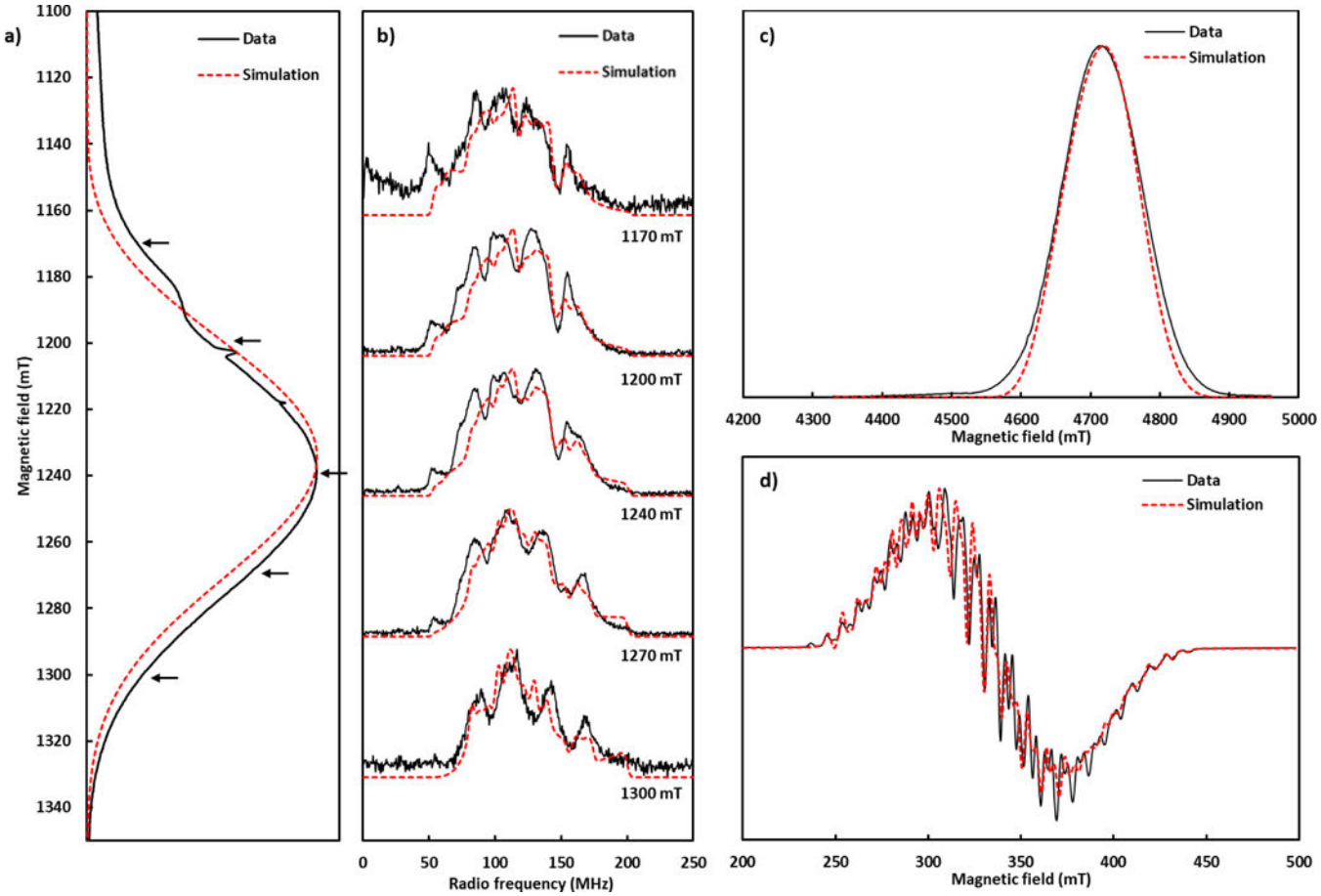

Figure 8.

Experimental spectra of **3-ox** (black traces) and simulation (dashed red traces). a) Q-band electron spin echo (ESE) EPR. b) Q-band ^{55}Mn Davies ENDOR recorded at five magnetic field positions indicated in a). Acquisition parameters: Temp. = 3.8 K, MW freq. = 34.115 MHz, π_{MW} = 40 ns, π_{RF} = 3 μs, t_{RF} = 2 μs, τ = 400 ns. c) D-band ESE-EPR. d) X-band CW EPR. Acquisition parameters: Temp. = 5 K, MW freq. = 9.359 MHz, power = 2 mW, modulation amplitude = 4 G. See Table 1 for global fit parameters.

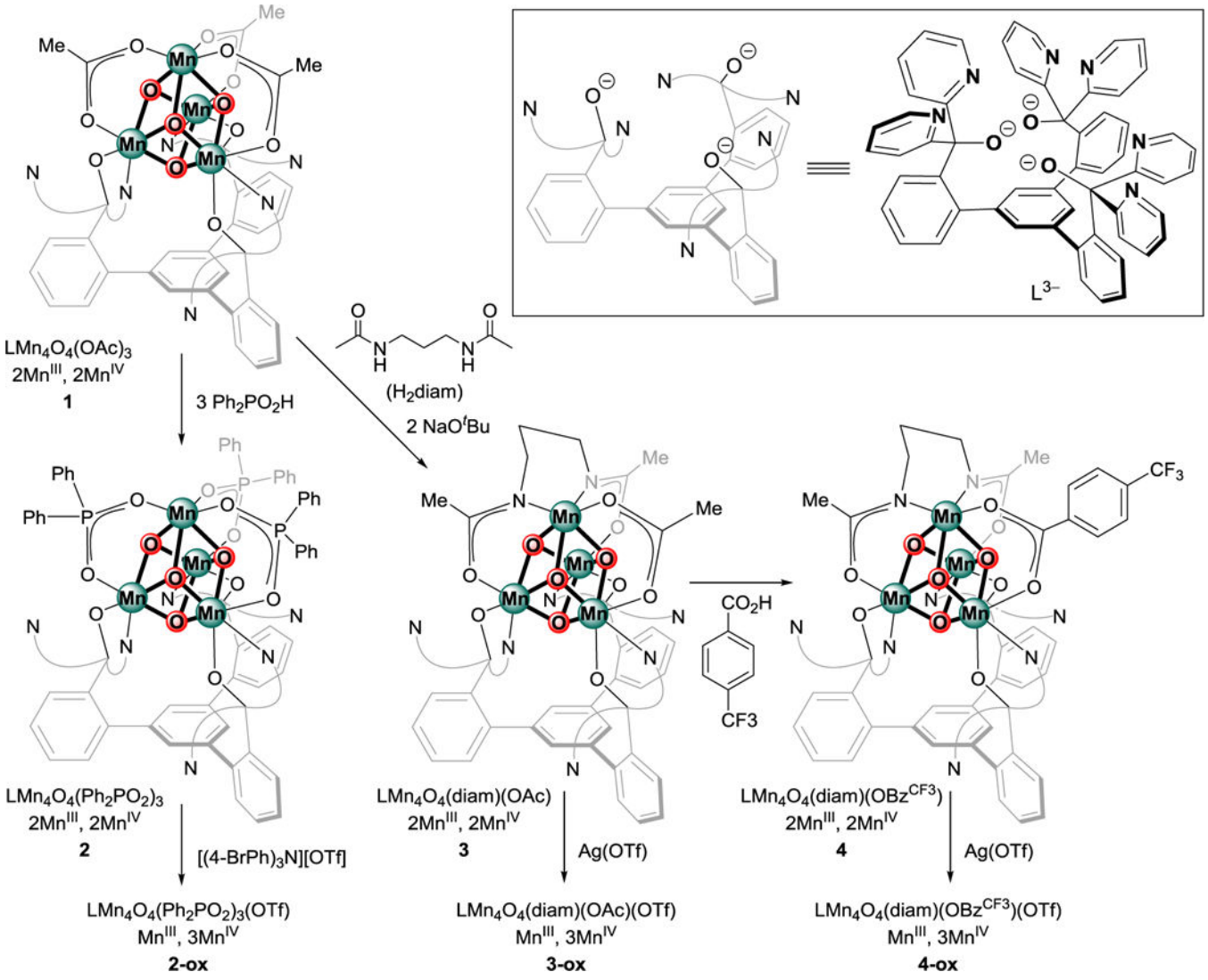

Scheme 1.

Synthesis of complexes **2**~**4** and their one-electron oxidized analogues **2-ox**~**4-ox**.

Table 1.

Summary of the effective *g* and ^{55}Mn HFI tensors for **3-ox**, and the S_2 states of *T. elongatus* and spinach PSII.[86, 97] Note: all hyperfine tensor frames collinear with *g*-tensor frame.

		g	**A_i (MHz)**			
			A_1	**A_2**	**A_3**	**A_4**
3-ox	x	1.944	376	233	253	193
	y	1.964	297	198	283	222
	z	2.002	272	260	149	131
	iso	1.970	315	230	228	198
T. elongatus	x	1.971	350	249	202	148
	y	1.948	310	227	182	162
	z	1.985	275	278	240	263
	iso	1.968	312	251	208	191
Spinach	x	1.997	310	235	185	170
	y	1.970	310	235	185	170
	z	1.965	275	275	245	240
	iso	1.977	298	248	205	193